Touchless Time-Varying Electrostatic Potential Sensing in Orbit: Fusion of X-ray and Electron Methods

Andrea López and Hanspeter Schaub

***Abstract*—Touchless determination of electrostatic potential is a foundational technology with diverse applications in orbital robotics, ranging from servicing missions to debris removal. This paper builds upon previous work that proposed the fusion of x-ray and electron sensing methods to remotely characterize the surface voltage of spacecraft. However, this study addresses dynamically varying electrostatic potentials, introducing a new approach to capture and adapt to time-varying potentials. The exploration of time-varying electrostatic potentials becomes increasingly vital as space missions evolve in complexity, emphasizing the need for adaptive sensing technologies. Vacuum chamber experiments are used to analyze and demonstrate the approach.**

***Index Terms*—Electrostatic potential, spacecraft charging, proximity operations, potential estimation, x-ray method, secondary electron method, Kalman filter.**

I. Introduction and Motivation

In the evolving landscape of space missions, the electrostatic potential of a target spacecraft is a variable parameter influenced by changing environmental conditions and mission dynamics. Electrical charging on satellite surfaces, induced by the space environment, can vary significantly over time as the spacecraft experiences different local space environments or changes its orientation. The resulting time-varying potentials can impact the safety and precision of proximity operations, satellite servicing, and debris removal. Additionally, accurate estimation of the time-varying potential is crucial in mission scenarios where active charge control is employed to ensure the effectiveness of the charge control system.

Understanding and monitoring time-varying electrostatic potentials is relevant in a spectrum of space missions. Although there are various methods available for assessing attributes like relative orientation and position, the options for remotely determining the electrostatic potential are limited. Bennett [1] explores charge estimation through relative motion dynamics using range and range rate measurements, providing a single charge measurement for the entire target and updating every few minutes. In contrast, Ferguson et al. [2] investigate techniques for monitoring charging or arcing events, such as surface glows, bremsstrahlung x-rays, and radio or optical emissions. They conclude that while ground-based telescopes might detect arcing, co-orbiting satellites are needed to sense the charge. This scarcity of methods for remote potential sensing is significant, given that electrostatic charging can lead to harmful arcing during contact or can considerably influence rendezvous dynamics through the introduction of disruptive forces and torques [3]. In scenarios involving proximity operations, where spacecraft navigate close quarters, the ability to comprehend the evolving electrostatic environment is essential for mission success.

The challenges of touchless time-varying electrostatic potential sensing are further compounded by the complexities of the space environment. The presence of plasma currents, solar radiation, and magnetic fields can introduce uncertainties and variations in the electrostatic potential of a spacecraft [4], [5]. This becomes particularly relevant in missions in geosynchronous orbits or the cislunar environment [6], [7], [8], where the spacecraft is exposed to a range of dynamic conditions and experiences varying levels of charging. Tracking the dynamic evolution of electrostatic potential of a target spacecraft is crucial for debris removal missions, particularly in the context of the electrostatic tractor concept [9], [10], [11], [12]. Here, real-time adaptability to changing potentials is necessary for controlled dynamics and electrostatic interactions without physical contact. The ability to adapt to these dynamic conditions is crucial for ensuring the reliability and accuracy of potential estimation methods.

This work combines two promising methods for remote potential sensing: the secondary electron method, or secondary electron emission or SEE method, and the x-ray method. The secondary electron method involves measuring the energy distribution of secondary electrons emitted from the target spacecraft, while the x-ray method involves measuring the energy of x-rays generated by the bremsstrahlung process at the target spacecraft. Prior work demonstrates the fundamental feasibility of each method for potential estimation in static scenarios [13], [14], [15], [16], [17], assuming the target potential is constant. The electron sensing method provides high accuracy but is sensitive to relative geometry, while the x-ray method, although less accurate, is more resilient to changes in target geometry. The fusion of these two methods was proposed in previous work to leverage the strengths of each method, aiming to mitigate individual limitations [18], by means of a Kalman filter. This study builds upon the previous work by exploring the fusion of x-ray and electron sensing methods for time-varying potentials. The fusion approach creates a more robust sensing suite capable of adapting to

A. López is a Graduate research Assistant at the Department of Aerospace Engineering Sciences, University of Colorado Boulder. E-mail: andrea.lopez@colorado.edu

H. Schaub is a Professor and Department Chair, Schaden Leadership Chair at the Department of Aerospace Engineering Sciences, University of Colorado Boulder.

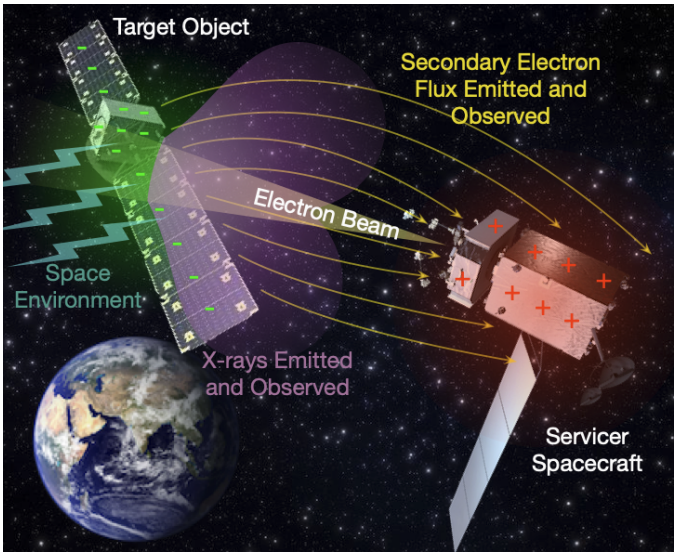

Fig. 1: Concept figure for touchless potential sensing. The figure shows the target spacecraft irradiated by the servicer's electron gun and the space environment, generating secondary electrons and x-rays. The secondary electrons and x-rays are detected by the servicer's sensors to estimate the target spacecraft's potential.

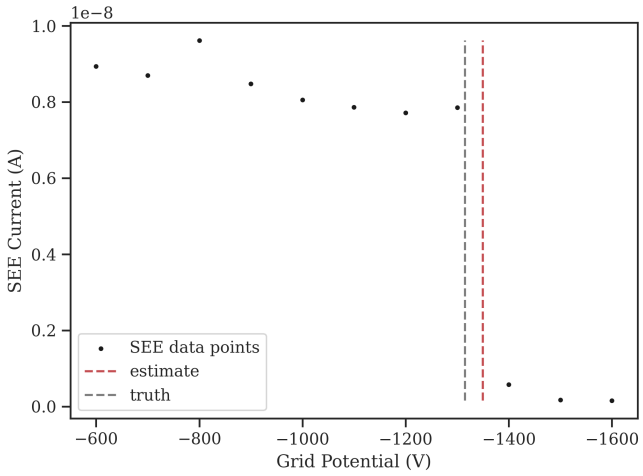

Fig. 2: Example of secondary electron current measured by an RPA. The figure shows the secondary electron current plotted against the grid potential of the RPA. The current drop in the secondary electron current curve corresponds to the potential of the target spacecraft.

dynamic electrostatic conditions.

This study considers an experimental approach designed to validate the proposed fusion method for scenarios with dynamically changing target potential to mimic the complexities of space missions. Both x-ray and electron sensing methods are employed concurrently to capture and analyze the time-varying electrostatic potentials of target spacecraft. The experimental data collected provides insights into the adaptability and accuracy of potential estimation methods in scenarios with dynamically changing potentials.

II. Review of Sensing Methods

A. Secondary Electron Method

As energetic electrons impact a surface, they can generate additional electrons through secondary emission. These secondary electrons are emitted from the surface at energies of a few eV. The number of secondary electrons emitted is dependent on the energy of the incident electron, the material properties of the surface, and the angle of incidence.

This method of remote sensing involves a servicer spacecraft with an active electron gun that may irradiate the target object, or be pointed off into space. By emitting energetic electrons, the servicer craft becomes positively charged. Secondary electrons originate from the target's surface, either due to the direct impact of the service craft's electron beam or from the ambient plasma currents present in the space environment. The electric field between the target and the positively charged servicer accelerates the secondary electrons towards the servicer, where they are observed with an electron energy analyzer. Electron energy analyzers are a commonly used instruments on spacecraft and have considerable flight heritage [19], [20], [21]. Because of the low emission energy of these secondary electrons, the energy of the electrons as observed by the servicer is approximately equal to the potential difference between the servicer and the target spacecraft. Thus, if the electric potential of the servicer is known, the potential of the target object can be inferred, with accuracies on the order of 10 V [14].

An example of the measured secondary electron current is shown in Figure 2, where the secondary electron current is plotted against the grid potential of a retarding potential analyzer (RPA). The potential of the target spacecraft can be estimated by locating the current drop in the secondary electron current curve, which corresponds to the potential of the target. In this example, the RPA grid voltage sweeps values from -600 V to -1600 V, with a step size of 100 V. The step size of the RPA defines the resolution of the potential estimation, with smaller step sizes providing higher resolution. Here, the measured current drops between -1300 V and -1400 V, with the resulting estimate of -1350 V.

However, although accurate, there are limitations to the secondary electron method. A sufficient number of secondary electrons must be generated from the target spacecraft and collected by the instrument to ensure signal detection against the broad spectrum ambient plasma background. Additionally, the electron trajectories depend on the electric field between the two craft, which is sensitive to the relative geometry and environmental conditions. For tumbling objects, for example, there will be relative attitudes where the secondary electron method is not effective, leading to significant gaps in the potential estimation. Prospects and challenges of using the secondary electron method for remote potential sensing discussed more extensively in Ref. [13].

B. X-ray Method

When an energetic electron interacts with the electric fields around an atomic nucleus, it experiences a deceleration. This

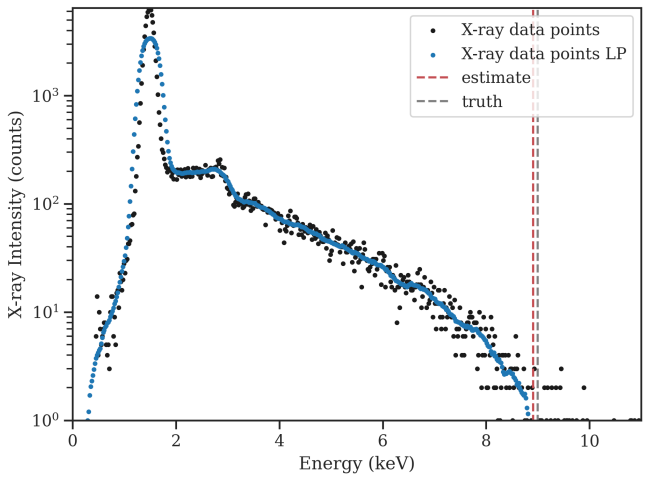

Fig. 3: Example of x-ray intensity measured by an x-ray spectrometer. The figure shows the x-ray intensity plotted against the energy of the x-rays. A low-pass (LP) filter is applied to the x-ray intensity to reduce noise. The maximum energy of the x-ray spectrum corresponds to the upper limit of the electron landing energy, which can be used to estimate the potential of the target spacecraft.

loss of kinetic energy results in the emission of x-rays in a continuous spectrum, in a process called bremsstrahlung. The kinetic energy of the incident electron (pre-deceleration) is referred to as the landing energy. The maximum energy that can be emitted by a single interaction corresponds to a complete deceleration of the electron, and is equal to the landing energy. If the initial energy of the electron is known (i.e., the emission energy from the electron gun, or the energy of the electrons in the ambient plasma), and the landing energy is measured, the change in energy can be used to estimate the difference in potential between the servicer and the target spacecraft.

The x-ray method involves the servicer spacecraft irradiating the target spacecraft with energetic electrons. The x-rays generated by the bremsstrahlung process are detected by an x-ray spectrometer at the servicer. This type of instrument has prior flight heritage, and has typical energy resolution on the order of 100 eV [22]. The energy of the x-rays is measured the spectrometer to estimate the landing energy of the electrons. An example of the measured x-ray intensity is shown in Figure 3, where the x-ray intensity is plotted against the energy of the x-rays. The potential of the target spacecraft can be estimated by locating the maximum energy of the x-ray spectrum, which corresponds to the upper limit of the electron landing energy. By subtracting the initial electron energy from the maximum energy of the x-ray spectrum, the difference in potential between the servicer and the target spacecraft can be estimated. In this example, the initial energy of the electrons is 10 keV, and the maximum energy of the x-ray spectrum is 8.91 keV, resulting in an estimate of -1090 V. The actual potential of the target spacecraft in Figure 3 is -1000 V.

The highest energy portion of the x-ray spectrum is noisy and can be difficult to resolve accurately [15], [17]. Additionally, the bremsstrahlung radiation has directional dependency, which impacts the accuracy of the measured landing energy. The accuracy of the x-ray method is on the order of 100 V [16]. Although less accurate than the secondary electron method, the x-ray method is more resilient to changes in target geometry and space environment, making it a complementary method for potential estimation.

III. Fusion of X-ray and Electron Sensing Methods

A. Preprocessing

The data collected by the instruments, RPA and x-ray spectrometer, was preprocessed to provide estimates of the potential of the target object, which were then used as inputs to the Kalman filter.

The RPA step size and measurement duration introduce discretization errors in the potential estimation. The midpoint in time and potential of each measurement are used as the potential estimates. For example, if the RPA sweeps from -400 V to -1600 V with a step size of 100 V in 100 seconds, and the current drop occurs between -1000 V and -1100 V, the potential estimate is -1050 V at second 50. The potential estimates from the RPA are shown in Figure 4, for a linear potential profile with an initial potential of -500 V and a rate of change of -1.0 V/s.

To mitigate the staircasing effect introduced by the RPA step size, a first-order low-pass filter is applied to the potential estimates, with a cutoff frequency of a fifth of the measurement rate. Assuming x is raw input and y is the filtered output, the Laplace domain description of the filter transfer function is

$$\frac{y}{x} = \frac{\omega_c}{s + \omega_c} \tag{1}$$

where ω_c is the critical cutoff frequency. The filtered potential estimates are shown in Figure 4, for the same linear potential profile. A well-known drawback of applying a low-pass filter is the introduction of a phase lag in the signal. In offline applications, the phase lag can be corrected by shifting the signal in time with a forward-backward filter. In online applications, the phase lag can be compensated for by using a small batch of data to estimate the phase lag and then applying the correction to the real-time data. For this study, the potential estimates used as inputs to the Kalman filter were not phase lag corrected.

The x-ray potential estimation is also affected by discretization errors in the time domain. The time associated with the x-ray potential estimate is the midpoint of the accumulation time.

Figure 5 shows the potential estimates from the RPA and x-ray spectrometer for the same linear potential profile and for a sinusoidal potential profile with an initial potential of -1000 V, an amplitude of 500 V, and an angular speed of 1 deg/s. The potential estimates from the secondary electron method are shown with the low-pass filter applied, for RPA steps of 100 V. Here, the phase lag introduced by the low-pass filter is evident in the potential estimates. These potential measurements are used as inputs to the Kalman filter to estimate the time-varying potential of the target spacecraft.

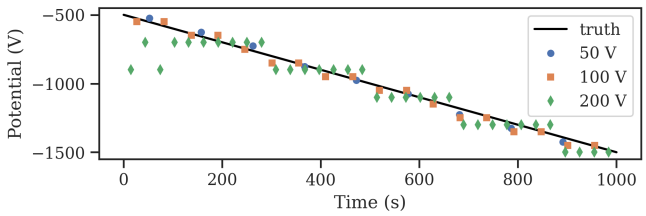

(a) Raw measurements

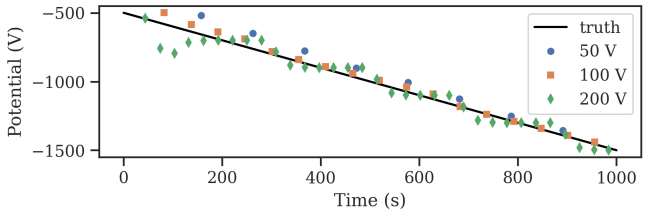

(b) LP-filtered measurements

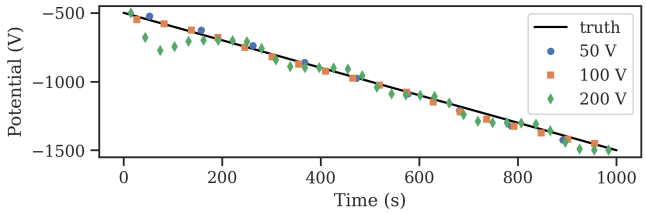

(c) Forward-backward LP-filtered measurements

Fig. 4: Filtered potential estimates from the secondary electron method for a linear potential profile with an initial potential of -500 V and a rate of change of -1.0 V/s. This figure illustrates the effect of the low-pass filter on the potential estimates.

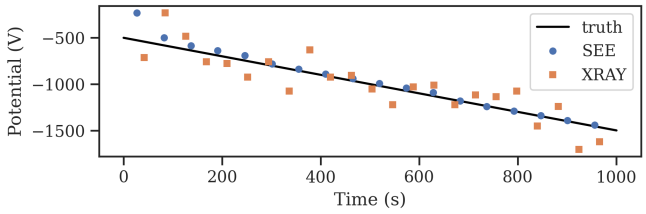

(a) Linear potential profile

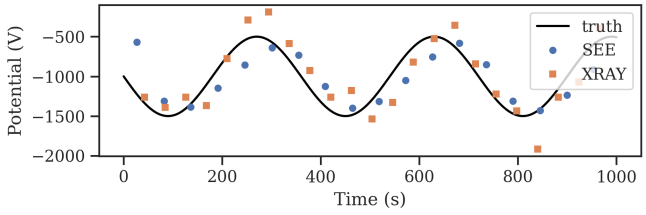

(b) Sinusoidal potential profile

Fig. 5: SEE and x-ray measurements for the linear and sinusoidal potential profiles, after preprocessing. The SEE potential estimates are shown with the low-pass filter applied.

B. Kalman Filter Algorithm

The secondary electron method and the x-ray method have their own strengths and limitations for potential estimation, as discussed in the previous sections. The secondary electron method provides high accuracy but is sensitive to relative geometry, while the x-ray method is more resilient to changes in target geometry but is less accurate. The fusion of the two methods aims to leverage the strengths of each method to mitigate individual limitations. The Kalman filter algorithm is used to estimate the potential of the target spacecraft from the potential estimates provided by the RPA and x-ray spectrometer. The Kalman filter is a recursive algorithm that estimates the state of a dynamic system from a series of noisy measurements [23]. The Kalman filter is widely used in spacecraft navigation and control applications, and has been applied to potential estimation in previous work [18]. The algorithm is described by two equations: the state prediction equation and the measurement update equation, and is summarized in Algorithm 1.

Algorithm 1 Kalman Filter Algorithm

Initialize filter with $\hat{x}_k^+ = x_0$ and $P_k^+ = P_0$ with $k = 0$
for $k = 1, 2, \ldots, N$ **do**
  ▷ *State prediction*
  Predict state: $\hat{x}_k^- = A\hat{x}_{k-1}^+$
  Predict error covariance: $P_k^- = AP_{k-1}^+A^T + Q$
  ▷ *Measurement update*
  if SEE measurement available **then**
    Compute measurement residual: $z_k^- = z_{SEE} - H\hat{x}_k^-$
    Compute Kalman gain: $K_k = P_k^- H^T (HP_k^- H^T + R_{SEE})^{-1}$
    Update state estimate: $\hat{x}_k = \hat{x}_k^- + K_k(z_k^- - H\hat{x}_k^-)$
    Update error covariance: $P_k = (I - K_k H)P_k^-$
  else if X-ray measurement available **then**
    Compute measurement residual: $z_k^- = z_{xray} - H\hat{x}_k^-$
    Compute Kalman gain: $K_k = P_k^- H^T (HP_k^- H^T + R_{xray})^{-1}$
    Update state estimate: $\hat{x}_k^+ = \hat{x}_k^- + K_k(z_k^- - H\hat{x}_k^-)$
    Update error covariance: $P_k^+ = (I - K_k H)P_k^-$
  else
    Update state estimate (no meas.): $\hat{x}_k^+ = \hat{x}_k^-$
    Update error covariance (no meas.): $P_k^+ = P_k^-$
  end if
end for

Constructing a dynamic model that accurately represents the time-varying potential of an arbitrary target object subject to the space environment and the impact of an electron gun is extremely challenging. Therefore, the state prediction equation used in the Kalman filter algorithm is greatly simplified for this study. Three different dynamic models were considered for the state prediction equation: a constant potential model (CP), a constant potential rate model (CR), and a constant potential acceleration model (CA). The constant potential model assumes that the potential of the target spacecraft remains constant over time. The constant potential rate model and the constant potential acceleration model assume that the potential of the target spacecraft changes linearly and quadratically over time, respectively. The dynamic model used for the state prediction equation impacts the accuracy of the potential estimation. To accommodate for the three dynamic models, the state vector x_k

is defined as $x_k = [V_k, \dot{V}_k, \ddot{V}_k]^T$, where V_k is the potential of the target spacecraft, and $\dot{V}_k$ and $\ddot{V}_k$ are the rate of change and acceleration of the potential, respectively. The state transition matrix A is defined for each dynamic model as follows:

$$A_{CP,k} = \begin{bmatrix} 1 & 0 & 0 \\ 0 & 0 & 0 \\ 0 & 0 & 0 \end{bmatrix}, \tag{2}$$

$$A_{CR,k} = \begin{bmatrix} 1 & \Delta t_k & 0 \\ 0 & 1 & 0 \\ 0 & 0 & 0 \end{bmatrix}, \tag{3}$$

$$A_{CA,k} = \begin{bmatrix} 1 & \Delta t_k & \frac{1}{2}\Delta t_k^2 \\ 0 & 1 & \Delta t_k \\ 0 & 0 & 1 \end{bmatrix}, \tag{4}$$

where $\Delta t_k = t_{k+1} - t_k$ is the time step between steps k and $k+1$. Effectively, the CP model is a piecewise constant estimate of the potential, which is equivalent to the assumption that the potential remains constant over time used in prior work.

The process noise model used in the Kalman filter is a state noise compensation model, with a process noise covariance matrix $Q = \text{diag}[1, 0.001, 0.00001]\Delta t_k$. The measurement noise covariance matrix for the secondary electron method $R_{SEE} = \sigma_{SEE}^2 = 100$ V, and for the x-ray method $R_{xray} = \sigma_{xray}^2 = 10000$ V. The measurement matrix H is defined as $H = [1, 0, 0]$. The initial state estimate $\hat{x}_0$ and error covariance P_0 are set to $\hat{x}_0 = [0, 0, 0]^T$ and $P_0 = \text{diag}[1000000, 100, 1]$. The Kalman filter algorithm is applied to the potential estimates from the RPA and x-ray spectrometer to estimate the time-varying potential of the target spacecraft.

IV. Experimental Setup

Prior work either investigated the feasibility of each of the two methods for potential estimation separately [13], [14], [15], [16], or considered the fusion of the two methods for static potentials [18]. This study is a natural extension of the previous work, exploring the fusion of x-ray and electron sensing methods for time-varying potentials. The experimental data was collected using the Electrostatic Charging Laboratory for Interactions between Plasma and Spacecraft (ECLIPS) vacuum chamber [24] at the University of Colorado Boulder. Figure 6 shows the experimental setup used to capture the time-varying potentials of a target spacecraft. A Kimball Physics EGM-4212 electron gun was used to irradiate an aluminum cube that represents the target spacecraft, generating secondary electrons and x-rays. The potential of the aluminum cube was varied using a Matsusada AU-30R1 High-Voltage Power Supply (HVPS) with a prescribed time-varying profile. A custom-built retarding potential analyzer (RPA) was used to measure the secondary electron current, and an Amptek X-123 x-ray spectrometer with a Si-PIN detector was used to measure the x-ray intensity. The data from the RPA and x-ray spectrometer were collected simultaneously to capture the time-varying potentials of the target spacecraft.

Three sets of experiments were conducted to validate the fusion method for time-varying potentials. The first set of

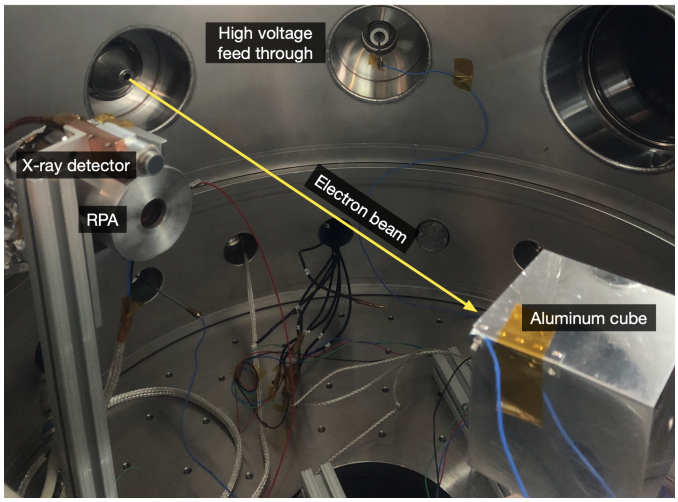

Fig. 6: Experimental setup for capturing time-varying potentials of a target spacecraft. The figure shows the electron gun irradiating the aluminum cube, generating secondary electrons and x-rays. The secondary electrons and x-rays are detected by the RPA and x-ray detector, respectively, to estimate the target spacecraft's potential.

experiments involved a linear variation of the potential of the cube, following the equation

$$V(t) = V_0 + \dot{V}t, \tag{5}$$

where $V_0 = -500$ V is the initial potential, $\dot{V} = -1.0$ V/s is the rate of change of potential, and t is the time.

The second set of experiments prescribed a sinusoidal variation of the potential of the cube, following the equation

$$V(t) = V_0 + A\sin(\omega t), \tag{6}$$

where $V_0 = -1000$ V is the initial potential, $A = 500$ V is the amplitude of the sinusoidal potential, $\omega = 1$ deg/s is the angular speed, and t is the time. This set of experiments represents the scenario in which the target spacecraft is differentially charged and rotating at 1 deg/s as seen from the servicer spacecraft. The third set of experiments conducted used the same prescribed sinusoidal potential profile as the second set, but with a different angular speed of $\omega = 0.5$ deg/s.

These three sets of experiments were conducted with an electron gun energy of 10 keV and current of 1 μA. The RPA was set to sweep potentials from -400 V to -1600 V with steps sizes of 50 V, 100 V and 200 V for each experiment. The implication of the step size is that the RPA is unable to resolve the potential of the target spacecraft with accuracies finer than the step size. The step size of the RPA also defines the measurement acquisition rate, which is the time it takes to sweep through the entire potential range. The chosen step sizes strike a good balance between the resolution of the potential estimation and the acquisition rate. The x-ray spectrometer accumulation time was set to 20 seconds for all experiments. The sampling parameters and the cutoff frequencies of the low-pass filter applied to the SEE measurements are summarized in Table I.

TABLE I: Measurement parameters for the three sets of experiments.

Measurement	Step size (V)	Sampling int. (s)	Cutoff freq. (Hz)
SEE	50	105	0.0019
SEE	100	55	0.0036
SEE	200	29	0.0069
X-ray	-	42	-

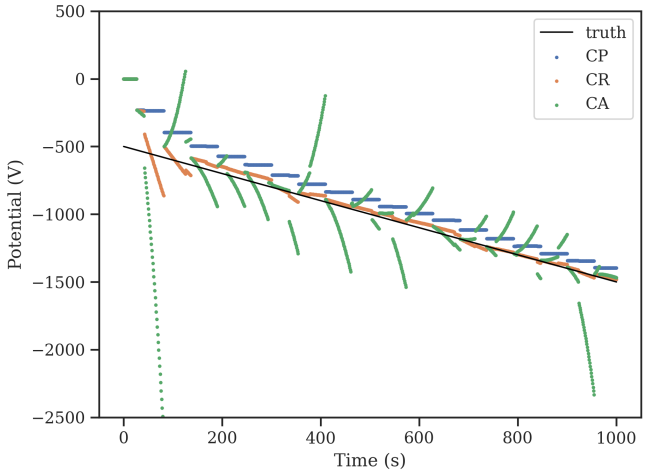

Fig. 7: Potential estimates from the Kalman filter for the three dynamic models and for the linear potential profile with an initial potential of -500 V and a rate of change of -1.0 V/s.

The duration of each experiment was 1000 seconds. The data collected from the RPA and x-ray spectrometer were pre-processed and used as inputs to the Kalman filter to estimate the time-varying potential of the target spacecraft.

V. Results

A. Linear Potential Profile

The potential estimates from the Kalman filter are shown in Figure 7 for the three dynamic models (constant potential CP, constant potential rate CR, and constant potential acceleration CA) and for the linear potential profile with an initial potential of -500 V and a rate of change of -1.0 V/s.

Figure 8 shows the errors in the potential estimates from the Kalman filter for each dynamic model. The errors are defined as the difference between the estimated potential and the true potential of the target spacecraft. As an additional metric for performance, the root-mean-square error (RMSE) after second 300 is calculated for each dynamic model. The RMSE for the CP model, the CR model, and the CA model are 98.87 V, 23.44 V, and 213.62 V, respectively. These results confirm that the CA model provides the worst performance in terms of potential tracking accuracy, as small deviations in the potential rate and acceleration can lead to large errors in the potential estimation. As expected, the CR model provides the best performance in terms of potential tracking accuracy, because the filter dynamic model corresponds with the prescribed potential profile. The CP model assumes that the potential

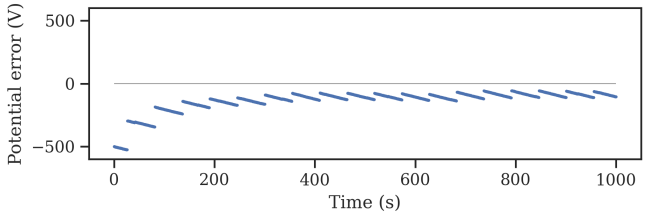

(a) CP model

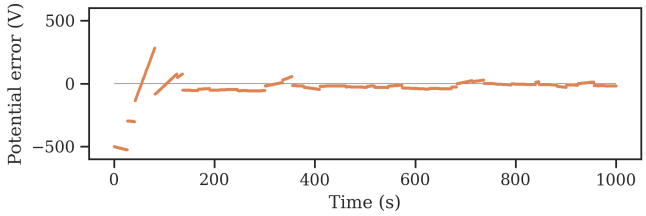

(b) CR model

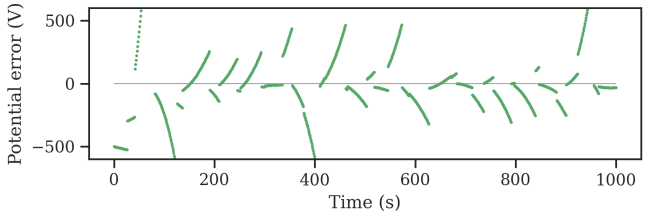

(c) CA model

Fig. 8: Errors in the potential estimates from the Kalman filter for the three dynamic models and for the linear potential profile with an initial potential of -500 V and a rate of change of -1.0 V/s.

is constant over time, which results in a piecewise constant estimate of the potential.

The scenario described above is an idealized case where the acquisition of measurements is uninterrupted for the duration of the experiments. In practice, measurement gaps can occur due to the relative geometry between the servicer and the target spacecraft, or other environmental factors. This is particularly relevant for the secondary electron method. To simulate measurement gaps, the potential estimates from the secondary electron method were removed on a periodic basis (i.e., x seconds on, x seconds off) with gaps of 100 seconds and 250 seconds. A case with no secondary electron measurements is also included for reference. These cases are illustrated in Figure 9. The potential estimates from the x-ray spectrometer were not removed, as the x-ray method is more resilient to changes in relative geometry and space environment. The potential estimates from the Kalman filter using the CR model are shown in Figure 10 for the linear potential profile, with measurement gaps of 100 seconds and 250 seconds, and only x-ray measurements. The RMSE after second 300 is calculated for each case. The RMSE for the case with 100-second gaps, 250-second gaps, and no SEE measurements are 90.42 V, 81.79 V, and 120.68 V, respectively. These results show that the Kalman filter is able to adapt to measurement gaps in the secondary electron method, and that the x-ray

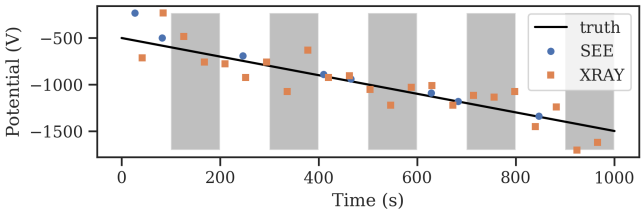

(a) 100-second gaps

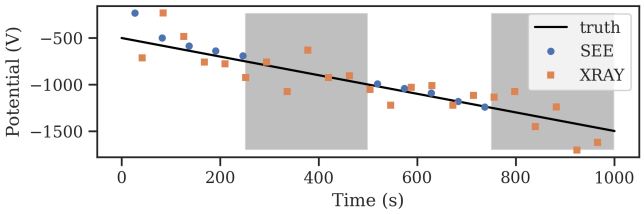

(b) 250-second gaps

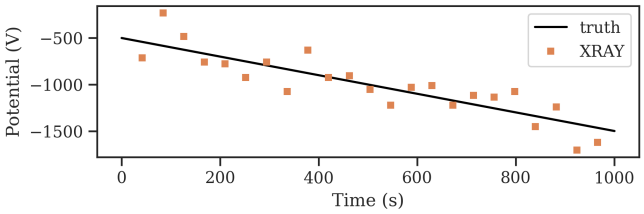

(c) No SEE measurements

Fig. 9: Potential measurements for the linear potential profile with an initial potential of -500 V and a rate of change of -1.0 V/s, with different SEE measurement gaps, or no SEE measurements. The greyed out regions in (a) and (b) indicate the SEE measurement gaps.

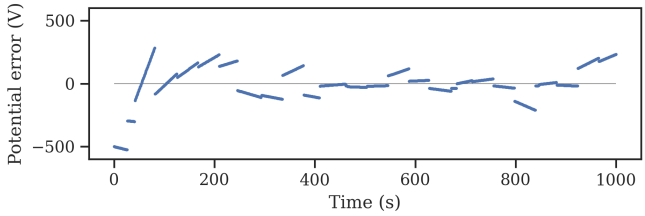

(a) 100-second gaps

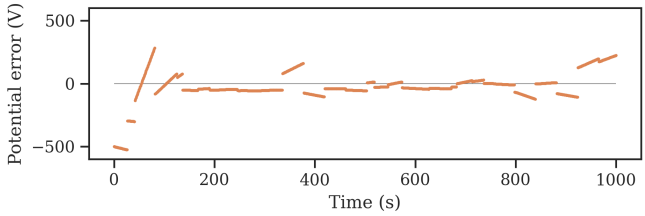

(b) 250-second gaps

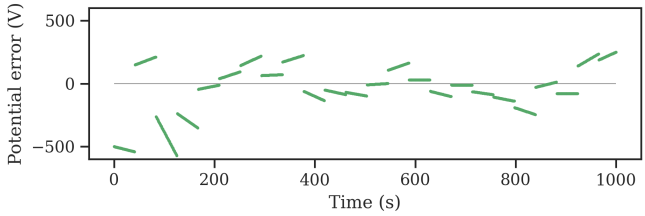

(c) No SEE measurements

Fig. 10: Potential estimates from the Kalman filter for the linear potential profile with an initial potential of -500 V and a rate of change of -1.0 V/s, with different SEE measurement gaps, or no SEE measurements.

method provides a complementary, less accurate measurement source for potential estimation. When available, the secondary electron measurements contribute to a more accurate potential estimate, decreasing the error noticeably. In the absence of secondary electron measurements, the x-ray method is able to provide a reasonable estimate of the potential of the target spacecraft.

B. Sinusoidal Potential Profile

The potential estimates from the Kalman filter for the three dynamic models are shown in Figure 11. These estimates correspond to a sinusoidal potential profile with an initial potential of -1000 V, an amplitude of 500 V, and an angular speed of 1 deg/s. The errors in these potential estimates for each dynamic model are displayed in Figure 12. The RMSE after 300 seconds is calculated for each dynamic model, yielding values of 399.54 V for the CP model, 278.49 V for the CR model, and 234.23 V for the CA model. Clearly, this fast changing potential profile is not well captured by the CP model, which assumes a constant potential. The CR model, which assumes a constant rate of change in potential, presents and improvement in performance, and so does the CA model, which assumes a constant acceleration in potential. However, Figure 11 shows how the Kalman filter estimates are lagging behind the true potential. This is a consequence of both the phase lag introduced by the low-pass filter, and the inadequacy of the dynamic models to represent the true potential profile.

For a slower sinusoidal profile, with an angular speed of 0.5 deg/s, the potential estimates from the Kalman filter show significant improvement. Figure 13 shows the potential estimates for the three dynamic models. The errors in these potential estimates are displayed in Figure 14. The RMSE after 300 seconds is calculated for each dynamic model, with values of 301.03 V, 135.91 V, and 169.80 V for the CP model, CR model, and CA model, respectively. This case presents a reduction in the RMSE values of 50% with the CR model compared to the previous case.

Figure 13 clearly shows that the Kalman filter estimates are lagging behind the true potential, also for this slower case. To assess the impact of the phase lag in the potential estimates, the SEE measurements were corrected for phase lag using a forward-backward low-pass filter. The potential estimates from the Kalman filter for the three dynamic models are shown in Figure 15. The errors for the CR model are displayed in Figure 16. The RMSE after 300 seconds is calculated for the CR model, yielding a value of 44.24V. This result shows a significant improvement in the potential tracking accuracy when the phase lag is corrected.

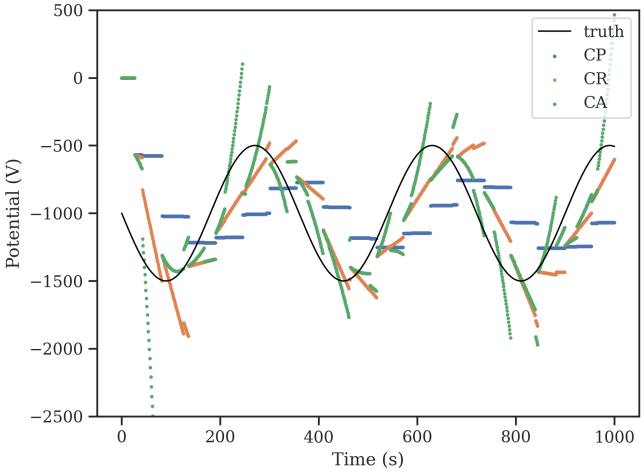

Fig. 11: Potential estimates from the Kalman filter for the three dynamic models and for the sinusoidal potential profile with an initial potential of -1000 V, an amplitude of 500 V, and an angular speed of 1 deg/s.

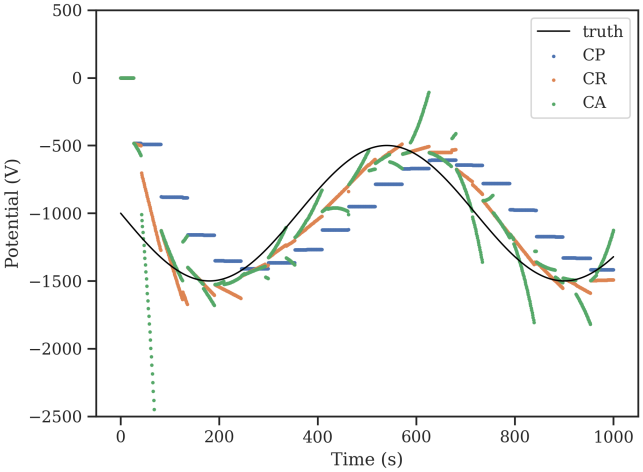

Fig. 13: Potential estimates from the Kalman filter for the three dynamic models and for the sinusoidal potential profile with an initial potential of -1000 V, an amplitude of 500 V, and an angular speed of 0.5 deg/s.

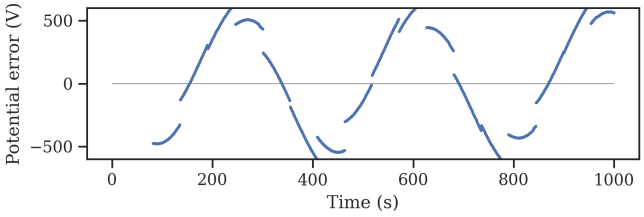

(a) CP model

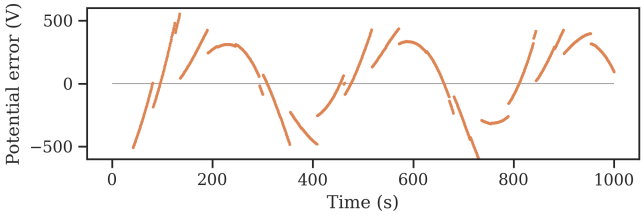

(b) CR model

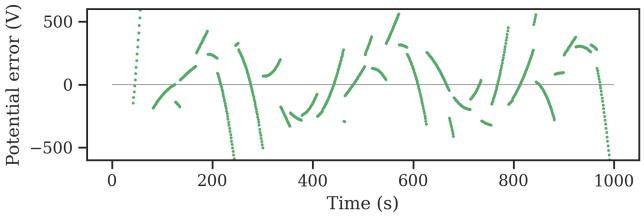

(c) CA model

Fig. 12: Errors in the potential estimates from the Kalman filter for the three dynamic models and for the sinusoidal potential profile with an initial potential of -1000 V, an amplitude of 500 V, and an angular speed of 1 deg/s.

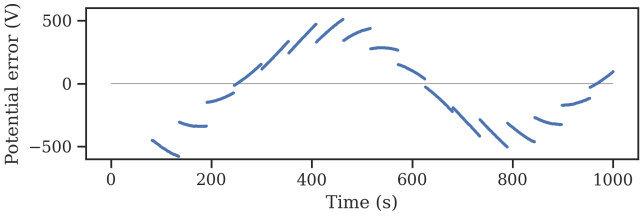

(a) CP model

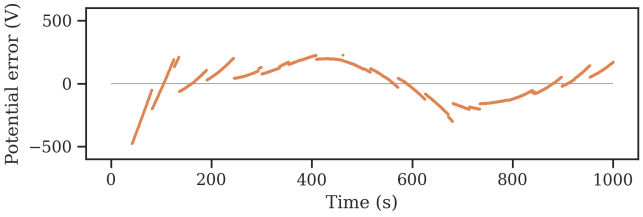

(b) CR model

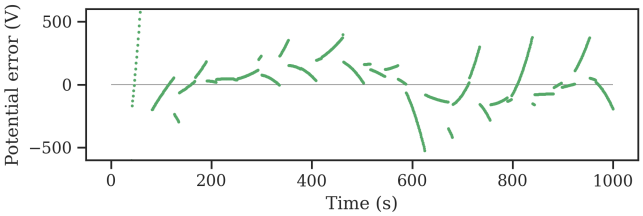

(c) CA model

Fig. 14: Errors in the potential estimates from the Kalman filter for the three dynamic models and for the sinusoidal potential profile with an initial potential of -1000 V, an amplitude of 500 V, and an angular speed of 0.5 deg/s.

Under the current experimental conditions and measurement rates, the CR model provides the best performance in terms of potential tracking accuracy for the sinusoidal potential profile. The case with a sinusoidal profile and angular speed of 1 deg/s is particularly challenging, as the potential changes rapidly over time and the measurement rates are not sufficient to

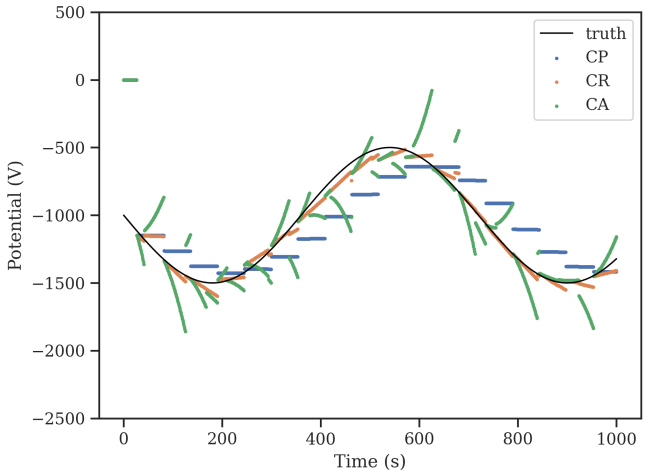

Fig. 15: Potential estimates from the Kalman filter for the three dynamic models and for the sinusoidal potential profile with an initial potential of -1000 V, an amplitude of 500 V, and an angular speed of 0.5 deg/s. The SEE measurements used as inputs to the Kalman filter have been corrected for phase lag.

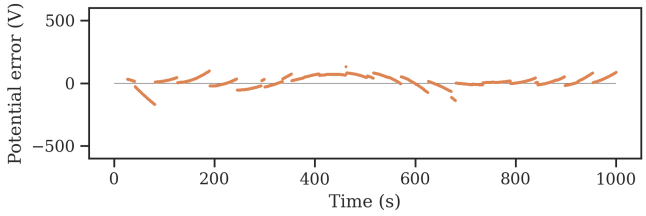

Fig. 16: Errors in the potential estimates from the Kalman filter for the CR model and for the sinusoidal potential profile with an initial potential of -1000 V, an amplitude of 500 V, and an angular speed of 0.5 deg/s. The SEE measurements used as inputs to the Kalman filter have been corrected for phase lag.

capture the fast changes. For slower potential profiles, the CR model provides a reasonable estimate of the potential of the target spacecraft. The phase lag introduced by the low-pass filter impacts the accuracy of the potential estimates, and can be corrected using a forward-backward low-pass filter.

VI. Conclusion

This study explored the fusion of x-ray and electron sensing methods for time-varying potentials. The experimental data collected using the ECLIPS vacuum chamber at the University of Colorado Boulder was used to validate the fusion method for scenarios with dynamically changing target potential. The potential estimates from the RPA and x-ray spectrometer were preprocessed and used as inputs to the Kalman filter to estimate the time-varying potential of the target spacecraft. The results show that a constant potential rate model provides the best performance in terms of potential tracking accuracy, provided that the actual potential changes are sufficiently linear between measurements. Although the accuracy of the results is deteriorated in the absence of secondary electron measurements, the x-ray measurements maintain the potential estimates within reasonable bounds. The phase lag introduced by the low-pass filter, used to mitigate the staircasing effect of the RPA steps, impacts the accuracy of the potential estimates. Correcting the phase lag significantly enhances potential tracking accuracy, especially for sinusoidal potential profiles. The results of this study demonstrate the feasibility of the fusion method for time-varying potentials, and provide insights into the adaptability, accuracy and limitations of potential estimation methods in scenarios with dynamically changing potentials.

Acknowledgments

This work was supported through the Air Force Office of Scientific Research (AFOSR) under award number FA9550-23-1-0570. A. Lopez gratefully acknowledges the support of the Future Investigators in NASA Earth and Space Science and Technology (FINESST) program, and the support of Zonta International through the Amelia Earhart Fellowship.

References

[1] T. J. Bennett, "On-orbit 3-dimensional electrostatic detumble for generic spacecraft geometries," Ph.D. dissertation, University of Colorado at Boulder, 2017.

[2] D. C. Ferguson, J. Murray-Krezan, D. A. Barton, J. Dennison, and S. A. Gregory, "Feasibility of detecting spacecraft charging and arcing by remote sensing," Journal of Spacecraft and Rockets, vol. 51, no. 6, pp. 1907–1913, 2014.

[3] K. Wilson and H. Schaub, "Impact of electrostatic perturbations on proximity operations in high earth orbits," Journal of Spacecraft and Rockets, vol. 58, no. 5, pp. 1293–1302, 2021.

[4] S. T. Lai, Fundamentals of spacecraft charging: spacecraft interactions with space plasmas. Princeton University Press, 2012.

[5] J. R. Dennison, R. Hoffmann, and J. Abbott, "Triggering threshold spacecraft charging with changes in electron emission from materials," in 45th AIAA Aerospace Sciences Meeting and Exhibit, 2007, p. 1098.

[6] M. Denton, M. Thomsen, H. Korth, S. Lynch, J.-C. Zhang, and M. Liemohn, "Bulk plasma properties at geosynchronous orbit," Journal of Geophysical Research: Space Physics, vol. 110, no. A7, 2005.

[7] F. B. Leahy, "SLS-SPEC-159, Cross-Program Design Specification for Natural Environments (DSNE) Revision I," Tech. Rep., 2021.

[8] M. L. Goodman, A. Paez, E. M. Willis, A. M. DeStefano, and R. M. Suggs, "An analytic model for estimating the first contact resistance needed to avoid damaging esd during spacecraft docking in geo," in Applied space environments conference, no. M19-7319, 2019.

[9] H. Schaub and Z. Sternovsky, "Active space debris charging for contactless electrostatic disposal maneuvers," Advances in Space Research, vol. 53, no. 1, pp. 110–118, 2014.

[10] J. Hughes and H. Schaub, "Prospects of using a pulsed electrostatic tractor with nominal geosynchronous conditions," IEEE Transactions on Plasma Science, vol. 45, no. 8, pp. 1887–1897, 2017.

[11] M. Bengtson, K. Wilson, J. Hughes, and H. Schaub, "Survey of the electrostatic tractor research for reorbiting passive geo space objects," Astrodynamics, vol. 2, pp. 291–305, 2018.

[12] J. Hammerl and H. Schaub, "Effects of electric potential uncertainty on electrostatic tractor relative motion control equilibria," Journal of Spacecraft and Rockets, vol. 59, no. 2, pp. 552–562, 2022.

[13] M. Bengtson, J. Hughes, and H. Schaub, "Prospects and challenges for touchless sensing of spacecraft electrostatic potential using electrons," IEEE Transactions on Plasma Science, vol. 47, no. 8, pp. 3673–3681, 2019.

[14] M. Bengtson, K. Wilson, and H. Schaub, "Experimental results of electron method for remote spacecraft charge sensing," Space Weather, vol. 18, no. 3, p. e2019SW002341, 2020.

[15] K. Wilson and H. Schaub, "X-ray spectroscopy for electrostatic potential and material determination of space objects," IEEE Transactions on Plasma Science, vol. 47, no. 8, pp. 3858–3866, 2019.

[16] K. Wilson, M. Bengtson, and H. Schaub, "X-ray spectroscopic determination of electrostatic potential and material composition for spacecraft: Experimental results," Space Weather, vol. 18, no. 4, p. e2019SW002342, 2020.
[17] K. Wilson, J. Hammerl, and H. Schaub, "Using plasma-induced x-ray emission to estimate electrostatic potentials on nearby space objects," Journal of Spacecraft and Rockets, vol. 59, no. 4, pp. 1402–1405, 2022.
[18] K. Wilson, M. Bengtson, and H. Schaub, "Remote electrostatic potential sensing for proximity operations: Comparison and fusion of methods," Journal of Spacecraft and Rockets, vol. 59, no. 5, pp. 1425–1436, 2022.
[19] W. C. Knudsen, K. Spenner, J. Bakke, and V. Novak, "Pioneer venus orbiter planar retarding potential analyzer plasma experiment," IEEE Transactions on Geoscience and Remote Sensing, no. 1, pp. 54–59, 1980.
[20] C. Pollock, T. Moore, A. Jacques, J. Burch, U. Gliese, Y. Saito, T. Omoto, L. Avanov, A. Barrie, V. Coffey et al., "Fast plasma investigation for magnetospheric multiscale," Space Science Reviews, vol. 199, pp. 331–406, 2016.
[21] A. W. Case, J. C. Kasper, M. L. Stevens, K. E. Korreck, K. Paulson, P. Daigneau, D. Caldwell, M. Freeman, T. Henry, B. Klingensmith et al., "The solar probe cup on the parker solar probe," The Astrophysical Journal Supplement Series, vol. 246, no. 2, p. 43, 2020.
[22] Amptek. X-123 Si-PIN X-ray Detector. [Online]. Available: https://www.amptek.com/products/x-123-si-pin-x-ray-detector/
[23] G. Welch and G. Bishop, "An introduction to the kalman filter," 1995.
[24] K. Wilson, A. Romero-Calvo, M. Bengtson, J. Hammerl, J. Maxwell, and H. Schaub, "Development and characterization of the eclips space environments simulation facility," Acta Astronautica, vol. 194, pp. 48–58, 2022.